Anal. Chem. **2009,** *81,* 4241–4248

Optimized Transport Setup for High Repetition Rate Pulse-Separated Analysis in Laser Ablation−Inductively Coupled Plasma Mass Spectrometry

Helmut Lindner,*,†,‡ David Autrique,† Carmen C. Garcia,§ Kay Niemax,§ and Annemie Bogaerts†

Department of Chemistry Research Group for Plasma, Laser Ablation and Surface Modelling−Antwerp (PLASMANT), University of Antwerp, Universiteitsplein 1, B-2610 Wilrijk, Belgium, and ISAS−Institute for Analytical Sciences, University of Dortmund, Bunsen-Kirchhoff-Strasse 11, D-44139 Dortmund, Germany

An optimized laser ablation setup, proposed for high repetition rate inductively coupled plasma mass spectrometry (ICPMS) analyses such as 2D imaging or depth profiling, is presented. For such applications, the particle washout time needs to be as short as possible to allow high laser pulse frequencies for reduced analysis time. Therefore, it is desirable to have an ablation setup that operates as a laminar flow reactor (LFR). A top-down strategy was applied that resulted in the present design. In the first step, a previously applied ablation setup was analyzed on the basis of computational fluid dynamics (CFD) results presented by D. Autrique et al. (*Spectrochim. Acta, B* 2008, *63*, 257−270). By means of CFD simulations, the design was modified in such a way that it operated in the LFR regime. Experimental results demonstrate that the current design can indeed be regarded as an LFR. Furthermore, the operation under LFR conditions allowed some insight into the initial radial concentration distribution if the experimental ICPMS signal and analytical expressions are taken into account. Recommendations for a modified setup for more resilient spatial distributions are given. With the present setup, a washout time of 140 ms has been achieved for a 3% signal area criterion. Therefore, 7 Hz repetition rates can be applied with the present setup. Using elementary formulas of the analytical model, an upper bound for the washout times for similar setups can be predicted. The authors believe that the presented setup geometry comes close to the achievable limit for reliable short washout times.

Direct solid microanalysis using laser ablation (LA) in combination with inductively coupled plasma mass spectrometry (ICPMS) is a widely used technique for fast and powerful multielement determination of solid samples at trace and ultratrace concentration levels for a wide variety of sample types. The growing interest in LA as a sampling technique stems from the ability to ablate diverse materials ranging from conducting to nonconducting inorganic and organic compounds as solids or powders. Besides bulk analysis, the focusing characteristics of lasers permit sampling in small areas, so that localized microanalyses and spatial mappings are feasible.

Spatially resolved information is important for many areas including medicine, archeology, chemistry, geology, and environmental and materials sciences. Some examples are the depth-profiling analysis of ancient coins,[1] the location of uranium contamination in human hair,[2] the detection of inclusions in clean steal,[3] the protein-related element distributions on blot membranes,[4] or the investigation of cave deposits.[5] For such analyses, the signals arising from laser pulses need to be evaluated separately for position−pulse correlation. Accordingly, the signal from one laser pulse should not interfere with those from previous pulses. Therefore, the signal has to reach noise level before applying the next pulse. Since many laser pulses are needed for such an investigation, the analysis time can become quite long. It can be reduced by using a setup with a shorter washout time because in that case higher pulse frequencies can be applied. The signal contributions from previous laser pulses are reduced, and the sensitivity is increased.

A laser ablation setup consists of three relevant parts for particle transport: the ablation cell, a gas connector, and the tubing. In most cases ablation cells have a relatively large volume allowing the examination of samples of variable size. Consequently, in most ablation setups the characteristics of the ablation cell dominate the signal.[6,7] Often strong mixing takes place in these cells. The signal can then be described by the continuous stirred-tank reactor model (CSTR).[8] Different aspects for understanding and reduction of the washout time of the ablation cell

* To whom correspondence should be addressed. E-mail: helmut.lindner@ua.ac.be.

† University of Antwerp.

‡ Previously worked at the ISAS, University of Dortmund.

§ University of Dortmund.

(1) Sarah, G.; Gratuze, B.; Barrandon, J.-N. *J. Anal. At. Spectrom.* **2007**, *22*, 1163–1167.
(2) Elish, E.; Karpas, Z.; Lorber, A. *J. Anal. At. Spectrom.* **2007**, *22*, 540–546.
(3) Dubuisson, C.; Cox, A. G.; McLeod, C. W.; Whiteside, I.; Jowitt, R.; Falk, H. *ISIJ Int.* **2004**, *44* (11), 1859–1866.
(4) Polatajko, A.; Azzolini, M.; Feldmann, I.; Stuezel, T.; Jakubowski, N. *J. Anal. At. Spectrom.* **2007**, *22*, 878–887.
(5) Woodhead, J. D.; Hellstrom, J.; Hergt, J. M.; Greig, A.; Maas, R. *Geostand. Geoanal. Res.* **2007**, *31* (4), 331–343.
(6) Leach, A. M.; Hieftje, G. M. *Appl. Spectrosc.* **2002**, *56* (1), 62–69.
(7) Feldmann, I.; Koehler, C. U.; Roos, P. H.; Jakubowski, N. *J. Anal. At. Spectrom.* **2006**, *21*, 1006–1015.
(8) Lindner, H. Ph.D. Thesis, Technische Universität Dortmund, Germany, 2008.

10.1021/ac802627x CCC: $40.75
Published on Web 04/29/2009

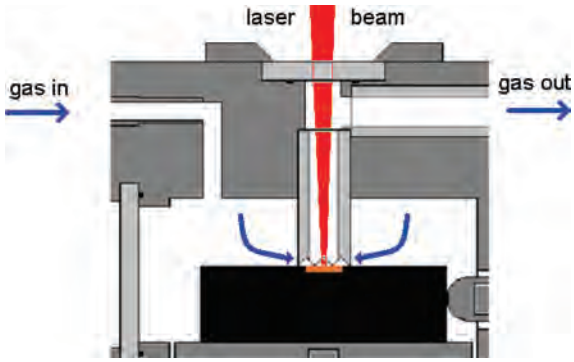

Figure 1. Scheme of the ablation cell used.

have been the subject of investigations. These are, for instance, the ablation cell volume,[6] different ablation positions in the cell,[9] and the effect of a nozzle at the inlet of the ablation cell.[10,11]

However, the ablation cell does not need to dominate the signal evolution. In the present study a sampling tube kind of ablation cell was used. It is similar to those described in refs 12 and 13 about 20 years ago. It consists of an outer cell of any volume and a tube for laser sampling; see Figure 1. The outer ablation cell provides space for the sample while the ablation takes place inside the sampling tube. Gas enters the sampling tube from the outer ablation cell and transports the ablated material to the ICP. Thus, the sampling tube is the only transport-relevant part of the cell. As a consequence, the transport tubing is the relevant part determining the washout time, as was demonstrated in ref 14. Furthermore, this type of ablation cell keeps its washout time constant for different positions of ablation in the outer ablation cell.[15] This allows analysis of large samples, without loss of sensitivity. It also provides short washout times compared to those of other ablation cells.[10] Nevertheless, also this kind of ablation cell needs further optimization to achieve the shortest particle washout time possible.

The actual setup under study here is based on that analyzed in ref 14 by means of computational fluid dynamics (CFD). The results of the simulation revealed that the route of transport dominates the signal. It was found that the ablation cell operated in a laminar regime but the transport tubing did not. Instead, turbulent regions and rotational flow structures were found in the gas connector and tubing used, resulting in considerable signal deterioration. The signals showed significant splitting and prolongation. Consequently, a laminar flow should be achieved throughout the transport, allowing use of the laminar flow reactor model (LFR). In the following section a strategy is compiled to modify the setup with the goal to further shorten the signal duration.

(9) Gurevich, E. L.; Hergenröder, R. *J. Anal. At. Spectrom.* **2007**, *22*, 1043–1050.
(10) Garcia, C. C.; Lindner, H.; Niemax, K. *Spectrochim. Acta, B* **2007**, *62*, 13–19.
(11) Bleiner, D.; Altorfer, H. *J. Anal. At. Spectrom.* **2005**, *20*, 754–756.
(12) Arrowsmith, P.; Hughes, S. K. *Appl. Spectrosc.* **1988**, *42* (7), 1231–1239.
(13) Uebbing, J.; Ciocan, A.; Niemax, K. *Spectrochim. Acta, B* **1992**, *47*, 601–610.
(14) Autrique, D.; Bogaerts, A.; Lindner, H.; Garcia, C. C.; Niemax, K. *Spectrochim. Acta, B* **2008**, *63*, 257–270.
(15) Garcia, C. C.; Lindner, H.; Niemax, K. *J. Anal. At. Spectrom.* **2009**, *24*, 14–26.

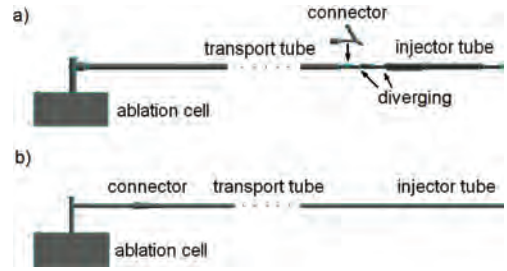

Figure 2. Scheme of (a) the previous[14] and (b) the new setups.

STRATEGY FOR ACHIEVING A REDUCED WASHOUT TIME

To optimize the setup of ref 14 for a shorter washout time, the following strategy consisting of three main steps was employed. In Figure 2 the previous[14] (a) and the new (b) setups are displayed.

The first step attempted to transform the flow regime in the tubing into an LFR regime. Regions where turbulences and rotational flows occurred (see ref 14) were altered in such a way that a laminar flow was realized throughout the tubing. This implies that diverging regions in the transport tube (cf. Figure 2) were avoided and a laminar gas connector was developed. As a result, the setup operates in the LFR regime. The connector is described in more detail below.

In the second step, the washout time of the setup was further reduced by increasing the flow velocity within the tube. This can be done in different ways. A first possibility consists of increasing the flow rate of the transport gas. Unfortunately, this was not possible in the present setup, since the pressure limit at the interface of the mass spectrometer was reached. Furthermore, different flow rates modify the residence time of the particles in the plasma and the plasma conditions. These can then strongly deviate from the optimum ones. Instead, the tube diameter was decreased down to the injector tube diameter, which results in a higher flow velocity within the tube without changing the plasma conditions. The injector tube exit diameter and the flow rates were the same as in the previous work[14] to have the same gas flow conditions at the ICP.

In the third step, the gas-adding connector was moved upstream. It was placed directly behind the ablation cell instead of being near the ICP injector tube (cf. parts a and b of Figure 2). In this way, the flow velocity is higher throughout a longer part of the transport tube but remains the same at the outlet of the injector tube.

For completeness, one has to mention that shortening of the transport tube length also results in shorter signals. Due to practical limitations, as in our case, or safety reasons this is not always possible. One could also think about mixing the gas before it enters the ablation cell. However, in that case the ablation conditions would be changed, which was to be avoided for the sake of comparison with the earlier experiment.[14] Nevertheless, it may be interesting to perform systematic studies to check whether improvements are possible by the proposed actions.

EXPERIMENTAL AND SIMULATION SETUP

A scheme of the ablation cell and the new transport arrangement are shown above in Figures 1 and 2b. A femtosecond laser beam (Hurricane, Spectra Physics, $\lambda = 795$ nm) was focused by

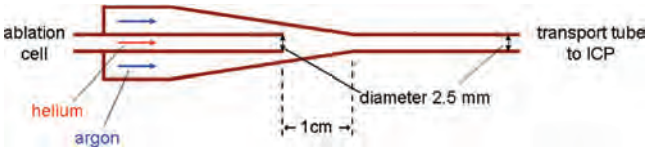

Figure 3. Gas connector providing laminar flows within the gas-adding region.

a lens ($f = 10$ cm) onto the sample. The pulse energy was set to 140 μJ, resulting in a central fluence of 10 J/cm^2 at the sample surface. The ablation cell depicted in ref 14 was used (see also Figure 1). The sampling tube had an inner diameter of 3 mm. The cell was flushed by helium with a flow rate of 1.2 L/min. A new gas connector (see below) was placed directly behind the sampling tube. For practical reasons the tube length between the sampling tube and the actual connector was 11 cm. Argon was added at the connector with a flow rate of 1.55 L/min. A 40 cm long transport tube was used to connect the setup to the ICP injector tube (12 cm long). The inner diameter of all tubes, except the sampling tube, was 2.5 mm. Therefore, diverging regions were avoided along the route of transport as discussed above. The mentioned flow rates are the same as in our earlier paper[10,14] given by the optimization procedure recommended in the manual of the ICP.

The ICP (HP4500, Agilent) was operated at a power of 1350 W, a plasma gas flow rate of 16 L/min of argon, and an auxiliary gas flow rate of 1.6 L/min of argon. The sample under study was brass (58% Cu, 40% Zn, and 2% Pb).

The simulations were performed using the CFD package Fluent (ANSYS). Detailed information on the simulation background is given in ref 14. Therefore, the CFD model is only briefly described here. For the simulations two geometries have been used. The first one was used to check for turbulences and rotational flow structures in critical tube parts, especially in the gas-connection zone (see below). This was done since a laminar flow regime was one goal for the new setup, as mentioned above. The tube behind the gas connector had a length of 6 cm, which was shorter than that later used in the experiment (see above). However, the Reynolds number of 300 clearly confirms a laminar flow for the not modeled tube part. The setup was divided into 4 million control volumes. The second geometry had the same dimensions as then applied in the experiment. The setup was divided into 6 million control volumes. With this setup, signals were simulated to compare with the experiment. For this purpose, 60 000 particle packages have been tracked using the discrete phase model (DPM). Their mass-size distribution was the same as in ref 14.

Connector for Laminar Flows. A new connector was developed on the basis of the CFD simulations. It consists of a frustrum-shaped outer tube and a straight inner tube; see Figure 3. The sample gas flows through the central tube, and the additional gas is introduced via the concentric frustrum tube. The inner diameter of the tube was 2.5 mm. To avoid turbulences at the end of the inner tube, the wall thickness of this tube has to be as small as possible. For the present setup the tube-wall thickness was 0.1 mm. The diameter change of the frustrum was 1.5 mm along a length of 20 mm.

The calculated turbulent intensity for flow rates of 1.2 L/min of helium (central tube) and admixed 1.55 L/min of argon

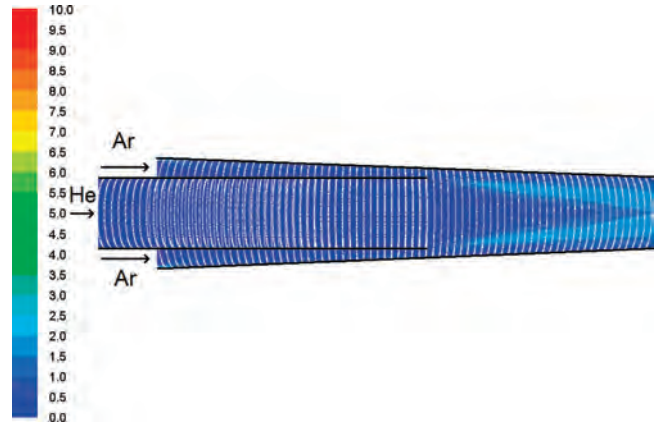

Figure 4. Calculated turbulent intensity (%) in the gas connector for He (central tube) and admixed Ar (frustrum tube) flow rates of 1.2 and 1.55 L/min, respectively.

(frustrum tube) are shown in Figure 4. As one can see, the flow behaves indeed nicely as a laminar flow.

THEORETICAL BACKGROUND

Laminar Flow Reactor Model. For experimental arrangements where the ablation cell is the dominating part, particularly for medium-sized ablation cells with a nozzle at the inlet,[10] the signal can approximately be described by a CSTR. Here, the material removed from the sample by the laser pulse is rapidly distributed in the ablation cell and the outflow is proportional to the material located inside the cell. The signal shows an exponential decay[16] with a time constant $\tau = V/\dot{V}$, where V is the (effective) volume and $\dot{V}$ is the flow rate.

However, not the ablation cell but the tubing is the part dominating the washout time in our experimental arrangement (see above). Changes in the setup (with respect to that described in ref 14) were performed to achieve a laminar flow as is illustrated above. Consequently, the flow in the tube can be described by the LFR model. In the LFR model the velocity profile is given by[16]

$$u = u_{\max}\left(1 - \frac{r^2}{R^2}\right) = 2u_{\text{mean}}\left(1 - \frac{r^2}{R^2}\right) = \frac{2\dot{V}}{A}\left(1 - \frac{r^2}{R^2}\right) \tag{1}$$

where $u_{\max}$, u_{mean}, R, and A are the maximum velocity, mean velocity, tube radius, and tube cross-section, respectively. Particles produced by femtosecond laser ablation are in a size range of about 10−500 nm.[17,18] For this size range and the regarded time scale, the particle transport can be assumed as size independent for a laminar flow.[19] This, together with eq 1, results in a signal profile of the form[16]

$$s(t) = s_0 \frac{2t_0^2}{(t_0 + t)^3} \tag{2}$$

(16) Baerns, M.; Hofmann, H.; Renken, A. *Chemische Reaktionstechnik*, 3rd ed.; Wiley-VCH: Weinheim, Germany, 2004.
(17) Koch, J.; von Bohlen, A.; Hergenröder, R.; Niemax, K. *J. Anal. At. Spectrom.* **2004**, *19*, 267–272.
(18) Koch, J.; Lindner, H.; von Bohlen, A.; Hergenröder, R.; Niemax, K. *J. Anal. At. Spectrom.* **2005**, *20*, 901–906.
(19) Baron, P. A.; Willeke, K. *Aerosol Measurements: Principles, Techniques and Applications*; John Wiley & Sons: New York, 2001.

where s_0 is the signal area, t the time after the signal start, and

$$t_0 = \frac{l}{u_{max}} \tag{3}$$

the (minimum) transit time of the material through the tube, where l is the tube length. At the time t_0 after material release, the signal starts (which refers to $t = 0$).

An interesting aspect is that the radial concentration distribution $C(r)$ remains unchanged during transport through the tube. As a result, one can write the signal for an arbitrary, axisymmetric concentration as

$$s'(t) = \frac{C(r)}{N} \frac{2{t_0}^2}{(t_0 + t)^3} \tag{4}$$

Here, s' denotes the area-normalized signal and N is the normalization factor. The transformation of $C(r)$ from the radial domain into the time domain can be calculated from

$$r^2(t) = R^2\left(1 - \frac{t_0}{t_0 + t}\right) \tag{5}$$

Washout Time of a Transport Tube at Laminar Flow Conditions. There are different ways for evaluating the washout time of an ablation setup. However, two main methods can be distinguished. In the first one, the signal width at a certain fraction of the maximum signal height is taken (e.g., half-width or 10%), while the second one determines the time from the ratio of an integral signal and the total signal area. For analytical purposes in ICPMS the authors prefer the latter definition since the amount of the analyte is proportional to the signal area. Here, the washout time t_{wA} is defined as the time at which only a certain fraction f_{SA} of material is still in the transport system. f_{SA} and t_{wA} for an LFR with an initially homogeneous radial analyte distribution are given by

$$f_{SA} = 1 - \frac{\int_0^{t_{wA}} s\,dt}{\int_0^{\infty} s\,dt} = \frac{{t_0}^2}{(t_0 + t_{wA})^2} \tag{6}$$

$$t_{wA} = t_0\left(\sqrt{\frac{1}{f_{SA}}} - 1\right) \tag{7}$$

If one applies the signal height criterion instead, the washout time t_{wH} and fraction f_{SH} are given by

$$f_{SH} = \frac{s(t{=}t_{wH})}{s(t{=}0)} = \left(\frac{t_0}{t_0 + t_{wH}}\right)^3 \tag{8}$$

$$t_{wH} = t_0\left(\sqrt[3]{\frac{1}{f_{SH}}} - 1\right) \tag{9}$$

Note that for the same washout time ($t_{wH} = t_{wA}$) the value for the height fraction is smaller than that for the area fraction. For example, a 10% height criterion corresponds to a 21.5% area criterion. This means that one calculates a shorter washout time (for $f_{SH} = f_{SA}$) with the signal height criterion than with the signal area criterion for the same setup. Therefore, an arrangement *seems* better using the height criterion.

Laminar Flow in Two Subsequent Tube Parts. In the present arrangement, as described above, the route of transport consists of two main parts: (i) from the sample surface to the gas connector and (ii) from the connector to the outlet of the ICP injector tube. As a consequence two elementary models for laminar tube transport are presented in this section. The first one assumes that the material is transported further on without being mixed in the region of the connector. In the second model, the material entering the connection region is instantaneously dispersed over the cross-section of the tube.

In the first model, the particles stay all at the same radial position from which they originated. The radial distribution is assumed to be homogeneous, and both tubes have the same diameter. The transport time as a function of the radius is given by the traveling times through each tube:

$$\begin{aligned} t'(r) &= t'_1(r) + t'_2(r) \\ &= \frac{l_1}{u_{max1}\left(1 - \frac{r^2}{R^2}\right)} + \frac{l_2}{u_{max2}\left(1 - \frac{r^2}{R^2}\right)} \\ &= \frac{t_{01} + t_{02}}{1 - \frac{r^2}{R^2}} \end{aligned} \tag{10}$$

Here, t_{01}, t_{02} and l_1, l_2 are the minimum transit times and lengths for tube parts one and two, respectively. The time t' after material release can also be written as $t' = t_{01} + t_{02} + t$, where t is the time after the signal start. From eq 10 follows

$$r^2(t) = R^2\left(1 - \frac{t_{01} + t_{02}}{t_{01} + t_{02} + t}\right) \tag{11}$$

The normalized signal is then given, with the derivation analogous to that given in ref 16 for a single tube, by

$$s'(t) = \frac{2(t_{01} + t_{02})^2}{(t_{01} + t_{02} + t)^3} \tag{12}$$

In the second model, the analyte annuli coming from the first tube are instantaneously spread into slices at the connection of the two tubes. Each slice produces a signal according to eq 2 for the second tube. Hence, a convolution needs to be carried out: The resulting signal can be understood as a superposition of the signals arising from the slices. The amount of material for each slice is determined by the first-tube signal (cf. eq 2). The intensity at the outlet of the second tube is an accumulation of the contributions of all signals which started before the actually regarded slice. The previous slices have a time distance of θ to the signal start of the first slice. Consequently, the actual slice has a maximum time difference which is denoted θ_{max}.

$$s'(t) = \int_0^{\theta_{max}} \frac{2{t_{01}}^2}{(t_{01} + \theta)^3} \frac{2{t_{02}}^2}{(t_{02} + \theta_{max} - \theta)^3}\,d\theta \tag{13}$$

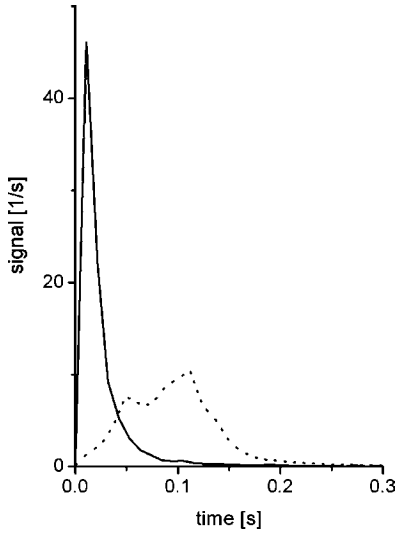

Figure 5. Area-normalized signals achieved by using the setup of ref 14 (dotted line) and the new setup (continuous line).

t_{01} and t_{02} are the minimum transport times for the first and the second tube parts, respectively. The result of eq 13 is given by

$$s'(t) = -4{t_{01}}^2{t_{02}}^2\left(\frac{6\left(\ln\left(\frac{t_{01}}{t_{01}+t}\right)+\ln\left(\frac{t_{02}}{t_{02}+t}\right)\right)}{(t_{01}+t_{02}+t)^5} - \frac{3\left(\frac{1}{t_{01}}+\frac{1}{t_{02}}-\frac{1}{t_{01}+t}-\frac{1}{t_{02}+t}\right)}{(t_{01}+t_{02}+t)^4} + \frac{\frac{1}{(t_{01}+t)^2}+\frac{1}{(t_{02}+t)^2}-\frac{1}{{t_{01}}^2}-\frac{1}{{t_{02}}^2}}{2(t_{01}+t_{02}+t)^3}\right) \quad (14)$$

As mentioned above, the time θ_{max} in eq 13 refers to the actual slice and is, therefore, the same as the signal onset time. Accordingly, it has been substituted by t in eq 14.

RESULTS AND DISCUSSION

Experimental Results. It is important to know the time evolution of a single signal if the ablated material arising from many subsequent laser pulses needs to be analyzed separately. The signal derived by the CFD simulations showed a strong improvement compared to the signal obtained with the arrangement studied in ref 14. Consequently, the experimental setup was built according to the simulated geometry, and measurements were performed. However, for descriptive reasons, the simulated signal will be displayed later. Only the measured characteristics are shown in this section.

The area-normalized experimental signal from the previous setup is displayed together with the new one in Figure 5. A total of 32 consecutive laser pulses were averaged to obtain the new signal. The time delay between two laser pulses was 1 s, which was sufficient to fully separate the signals (see below). The start time of the signals was determined by the null position of a straight line defined by the data point on the rising edge and the data point of the signal maximum. Subsequently, the data points of area-normalized signals were averaged.

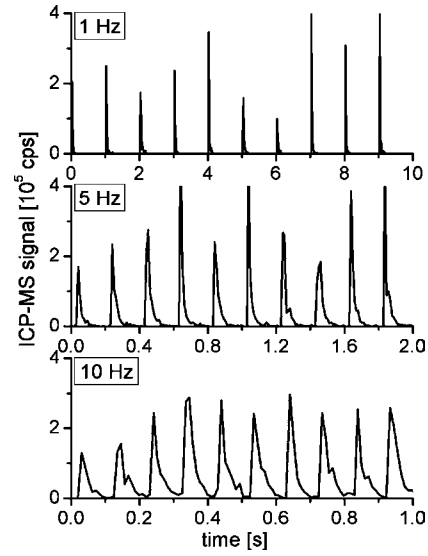

Figure 6. Multipulse signals with the new ablation setup at repetition rates of 1 Hz (top), 5 Hz (middle), and 10 Hz (bottom).

As one can see, the substructure which was present in the old signal is removed in the new signal. This indicates that the turbulent regions separating the particles[14] are indeed no longer present. The washout time, using a 3% area criterion, is now reduced from 230 to 140 ms. Hence, measurements need only 60% of the time, and a repetition rate of 7 Hz is applicable. Moreover, the washout time can further be reduced if more overlap is acceptable: the new signal has only a half-width of 16 ms, while the half-width was 95 ms for the old one. If one applies a 10% height criterion as in ref 9, the washout time of the present ablation arrangement is 45, with 165 ms for the previous one.

Multipulse signals obtained with laser repetition rates of 1, 5, and 10 Hz are presented in Figure 6 for the new setup. As one can see, the signals do not overlap for 1 and 5 Hz. For 10 Hz a small overlap is observable. However, the area contribution from the previous pulse is only about 4%. Since the washout fraction is not a definite value, it depends on the accuracy needed for the respective experiment whether one can apply this higher repetition rate or not.

Note that there are relatively strong signal fluctuations apparent in Figure 6. Besides the usual origins of fluctuations, one further important aspect has to be taken into account in the present case. The time resolution of the detector was only 10.5 ms. The signal rose to its maximum value within this time interval (see Figure 5). Hence, depending on the signal start and first data acquisition the signal height fluctuates for single pulses. This problem can be overcome by applying detectors with higher time resolution.

Theoretical Analysis of the Signal. The experimental signal obtained with the new setup is compared to the theoretical models for two purposes. The origin of the shape of the signal has to be understood better, and insight has to be gained to be able to transfer the results to similar arrangements when different parameters are applied. The applied models consist of the two analytical laminar models described above and the CFD model.

Analytical Models. In Figure 7 the experimental signal is presented together with the two analytical curves, in both linear and logarithmic scales. Here, the two transit times $t_{01} = 16$ ms

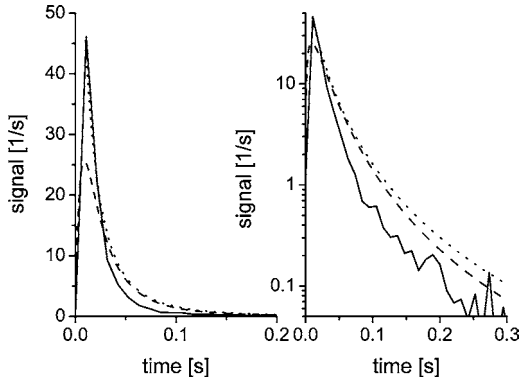

Figure 7. Experimental signal (full line) compared to that of the analytical models with (dashed line) and without (dotted line) mixing at the connector.

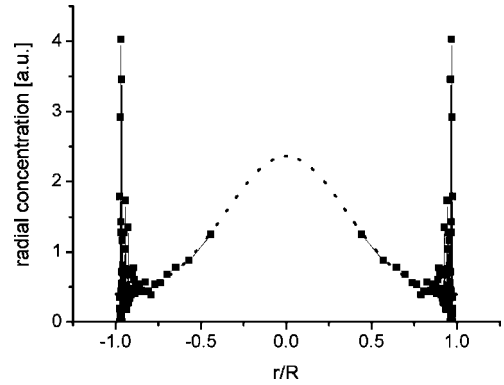

Figure 8. Radial concentration distribution calculated from the experimental signal. The signal has been mirrored (± signs from the square root of eq 5) at the $r = 0$ axis to provide a better view.

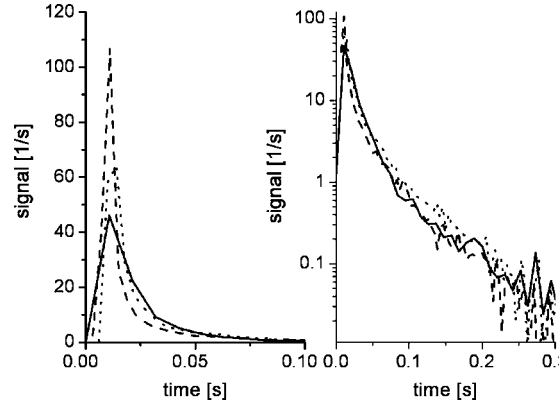

Figure 9. Comparison of experimental (full curve) and simulated signals with particle release at the sample surface (dashed line) and 2 mm above the sample surface (dotted line).

(from the sample to the gas admixture position) and $t_{02} = 28$ ms (from the gas admixture position to the injector outlet) were employed according to eq 3 and the applied parameters. No fitting parameters were used. The dotted curves refer to analytical model i where the material is assumed to remain on the same radial position (see eq 12). The dashed lines belong to analytical model ii where the material at the gas connector is assumed to be distributed across the cross-section of the tube (see eq 14).

One can see in the logarithmic scale graph of Figure 7 that the experimental signal line is curved. The decay follows, especially for later times, a t^{-3} dependence as expected for an LFR with a homogeneous mass distribution (see eq 4). As has been demonstrated above, the flow throughout the whole route of transport (tubes and connector) is laminar; i.e., no volumetric mixing region is present. Consequently, the signal decay was not exponential. This is different compared to experimental arrangements where a flow-effective volumetric ablation cell is used (see, e.g., ref 10). An exponential decay in the signal was also observed by applying the earlier experimental arrangement.[14] However, one can see in Figure 7 that the analytical models deviate considerably from the experimental signal. The decay observed in these models is too slow compared to the experimental one. The signal height of model i comes significantly closer to the experimental data, while it is about a factor of 2 smaller in the case of model ii. Therefore, the authors believe that model i is more realistic than model ii. This would mean that there is no strong mixing at the connector, which is supported by the laminar flow at the connector found by the CFD simulations above.

Radial Concentration Distribution. If one assumes that model i is applicable, one can deduce an initial relative radial mass distribution which would result in the measured signal. The radius r can be calculated from the time domain by applying eq 5. The calculated concentration distribution is determined by dividing the experimental signal by eq 12 and taking into account eq 4. The resulting radial concentration distribution is displayed in Figure 8. Note that the first data- point of the experimental signal has not been considered since its value is basically zero and the start position could not be determined exactly due to the poor time resolution of the ICPMS instrument (10.5 ms). The strong scatter near the tube wall ($r/R \approx \pm 1$) refers to the noise of the experimental signal at later times (low flow velocity; see eq 1) where the signal was already very low. In the central part of the tube only a few data points are present. This is again due to the relatively poor time resolution of the ICPMS instrument.

As can be seen in Figure 8, one finds a higher concentration of material in the center of the tube. This finding seems to be reasonable. A nearly homogeneous radial distribution with an excess in the center should be present if one takes the results of recent particle visualizations[20] into account. Furthermore, the expansion in femtosecond laser ablation has been found to be predominantly in the forward direction (see, e.g., ref 21). This also supports the finding that less material reaches the outer regions of the tube (cf. also Figure 1). However, since the resolution in the central part of the tube is very low, no definitive deduction of the real mass distribution can be made. Furthermore, some other effects take place and are regarded in the following.

Results of CFD Simulations. In contrast to the analytical models, the numerical simulation takes the whole setup geometry into account. In Figure 9 the experimental signal is displayed together with signals obtained by CFD simulations. In one case, the particles have been released from the sample surface (dashed line, case I), while they have been introduced 2 mm above the sample in the other case (dotted line, case II). A homogeneous mass distribution has been used across the cross-section of the tube in both cases.

(20) Koch, J.; Schlamp, S.; Rösgen, T.; Fliegel, D.; Günther, D. *Spectrochim. Acta, B* **2007**, *62*, 20–29.
(21) Albert, O.; Roger, S.; Glinec, Y.; Loulergue, J. C.; Etchepare, J.; Boulmer-Leborgne, C.; Perrière, J.; Million, E. *Appl. Phys. A* **2003**, *76*, 319–323.

First, only the two simulated signals are examined. The signal of case I is shorter than that of case II. This might be surprising since the distance to travel becomes shorter in the latter case. However, the change in the length of the route of transport is not significant compared to the whole distance—only a few millimeters with respect to about 60 cm. Therefore, that effect is negligible. However, there is another effect taking place. The gas flows from the side into the sampling tube. Therefore, material that is in this inlet region (as in case I) is transported into the center of the tube where the velocity is higher and results in a reduced dispersion. In case II the material is initially situated above the nooks of the sampling tube and therefore not pushed into the center of the tube. Note that case II is more realistic than case I: In ref 20 it is shown that after ablation most of the material is situated a few millimeters above the sample surface. Consequently, focusing of material by the inflowing gas at the sampling tube is considered as being relatively small.

Comparing the second case with experiment, one can see from the logarithmic scale graph that the decay fits relatively well. Therefore, a homogeneous mass distribution in the outer part of the tube is indicated. This is in line with the above finding using analytical model i to calculate the spatial distribution. However, there is one significant difference. For the fully homogeneous distribution, the analytical model predicts a too slow decay. This can be attributed to the fact that the gas connector has only been taken into account there in a simplified way. In fact, the added gas pushes the sample gas somewhat into the center of the tube, leading to a faster washout. The numerical simulation, on the other hand, takes that into account.

The early part of the simulated signal, however, does not fit with the experimental one. This can be attributed to a different initial spatial distribution of the material. One could try to adapt the distribution so that a signal comes out which corresponds to the experimental one. However, to achieve a physically meaningful prediction, at least 2D laser ablation modeling needs to be applied and coupled to Fluent. This is a challenging task and has to be done in the future.

REMARKS ON THE CALCULATION OF THE SPATIAL MASS DISTRIBUTION

Above, a radial mass distribution has been calculated from the experimental LA−ICPMS signal. However, the spatial resolution and accuracy of information which can be obtained with the present experimental arrangement are limited. Nevertheless, it presents a fast and easy method to gain information on spatial mass distributions after laser ablation which otherwise are only accessible with more sophisticated methods and arrangements.

A prerequisite for gaining information on the initial mass distribution is that an LFR regime is present within the whole transport. For instance, this is not possible when gas mixing takes place since the spatial information is lost in that case. An indication for that is an exponential decay of the signal (see the discussion of the CSTR above).

A primary assumption used in the model was radial symmetry. In ref 22, however, inhomogeneous particle distributions have been observed across the cross-section of the tube for laminar in-cell gas flows. Nevertheless, a radial symmetry can be assumed for the present setup due to the following fact. The transport geometry in ref 22 was different from the one used here. The ablation took place inside a cylindrical ablation cell, and the material was transported perpendicular to the ablation direction. In our case, the transportation was parallel to the ablation direction. The laser ablation plume can relatively well be regarded as axisymmetric to the ablation direction. This is of course not the case for the orthogonal direction, as has clearly been demonstrated in ref 20. Therefore, a more homogeneous radial distribution is to be expected in our case. However, still inhomogeneities occur. They can be reduced (as has been done) by averaging the signals of several laser pulses.

Unfortunately, it was not possible to achieve good insight into the material distribution in the center of the tube due to the poor time resolution (10.5 ms) of the ICPMS instrument. This can be improved by either increasing the time resolution of the detector or reducing the flow velocity within the tube. Here, one could increase the tube diameter if a torch with a respectively larger injector tube diameter is at hand. On the other hand, one could also lower the flow rate. However, in both cases, one has to take care of the changes of the ICP conditions.

In the previous section, it was deduced that the ablated material was pushed into the center of the tube at the gas connector. Although desired for short washout times, this is unfavorable for determining the spatial distribution. Consequently, no intermediate gas connector should be applied for such examinations. For the same reason, the height of gas-inlet nooks at the sampling tube should be smaller than the stopping distance of the material after laser ablation.

Changes in the tube diameter need to be avoided. Diverging parts lead to rotational flow structures and turbulences[14] and, consequently, to the loss of spatial information. Reductions of the tube diameter are better in that sense, but the recalculation of the distribution becomes more complicated due to the changes of the radial position of the material.

CONCLUSIONS

For LA−ICPMS the material to be analyzed is produced in an ablation cell and then transported to the ICP via a transport tube. The transport-relevant part of the ablation cell under study is basically only a tube. Thus, a prolongation of the signal arising from the actual ablation cell volume does not emerge. Turbulent regions and rotational flow structures within the route of transport prolonging the washout time[14] have been removed from the setup. An LFR regime has been achieved throughout the whole route of transport in the present experimental arrangement. Effects arising from transitional flows, although never completely evitable, can be regarded as minor since the actual Reynolds number of 300 is still much lower than 2300, the critical Reynolds number for turbulent flows in tubes. A higher mass concentration in the center of the tube has been observed, originating from the initial mass distribution and from added gas pushing the material to the center of the tube. Both effects are intrinsic of laser ablation and the setup geometry, respectively. They are desirable since they evoke an effective reduction of the washout time. Consequently, the signal predicted by simple analytical formulas was longer than the experimental one. Thus, the easy-to-use eqs 7 and 9 can be regarded as upper limits for the actual washout time. Only the

(22) Koch, J.; Wälle, M.; Dietiker, R.; Günther, D. *Anal. Chem.* **2008**, *80*, 915–921.

values of tube diameter, tube length(s), and gas flow rate(s) need to be known. The authors expect that only a reliable stronger focusing of the particles to the center of the tube could further shorten the washout time. Consequently, the authors believe that the actual setup comes close to the achievable limit for short washout times.

The present arrangement provides a washout time of 140 ms, allowing single-pulse analyses with a 7 Hz laser repetition rate. However, instruments providing higher time resolution than the present one are strongly recommended for achieving accurate analytical results, and the signal area instead of the signal height should be measured for data evaluation.

Furthermore, the present setup reveals some insight into the radial analyte distribution shortly after material expansion. However, the setup needs to be improved with regard to that purpose to achieve more accurate results. Especially, a gas admixture after the ablation cell should be avoided, and a faster detector should be used.

ACKNOWLEDGMENT

We are grateful to colleagues at the ISAS workshop for building the ablation cell and the gas connector. Funding by the Flemish Fund for Scientific Research (FWO Vlaanderen) and by the Deutsche Forschungsgemeinschaft (DFG) is also gratefully acknowledged. Further financial support was provided by the Federal Services for Scientific, Technical and Cultural Affairs (DWTC/SSTC) of the Prime Minister's Office through IUAP-VI and the Ministry of Innovation, Science, Research, and Technology of the state Northrhine-Westphalia as well as the Ministry of Education and Research of the Federal Republic of Germany. We are also thankful for the possibility to perform the calculations on the CALCUA supercomputer system of the University of Antwerp.

Received for review December 12, 2008. Accepted April 7, 2009.

AC802627X